Irrigation and Drainage Systems (2005) 19: 285–299 © Springer 2005

High density NOAA time series of ET in the Gediz Basin, Turkey

AMBRO GIESKE[1] & WOUTER MEIJNINGER[2]
[1]*ITC, International Institute for Geo-Information Science and Earth Observation, Water Resources Division, P.O. Box 6, 7500 AA Enschede, The Netherlands; E-mail: gieske@itc.nl*
[2]*Wageningen University, Meteorology and Air Quality Group, Duivendaal 2, 6701 AP Wageningen, The Netherlands*

Abstract. An evapotranspiration method comparison was carried out by the International Water Management Institute (IWMI, Sri Lanka), at two locations in the Gediz Basin, Turkey, in the period from May to September 1998. In the IWMI study a number of ground-based techniques were compared with results obtained by remote sensing methods. Recently, a search of the satellite active archive yielded over 70 high quality level 1b images from NOAA/AVHRR over the same time period. The processing of these images with the SEBAL algorithm enabled us to build up a detailed time series of sensible and latent heat fluxes for a period of 120 days. In this paper a comparison is made between the sensible and latent heat fluxes determined from the present series of NOAA-14/AVHRR images and the results obtained earlier from various other prediction methods applied during the 1998 IWMI project. Specifically, the NOAA/SEBAL results are assessed against the scintillometer and temperature fluctuation methods. The results show that the NOAA derived evapotranspiration values follow the seasonal irrigation cycle quite well and correspond closely to the Landsat derived values, although they are lower than the results obtained with the traditional crop factor and Penman–Monteith methods.

Key words: remote sensing, NOAA, Landsat, SEBAL, irrigation, evapotranspiration, scintillometer

Introduction

The International Water Management Institute (IWMI) brought researchers together in the Gediz Basin, Turkey, in 1998 to carry out a comparison between eight different methods to evaluate actual evapotranspiration. These included both field and remote sensing methods. The results and conclusions of this study were published in a special issue of the Journal of Hydrology (Kite & Droogers, 2000). While testing some technical issues relating to both remote sensing (Gieske, 2003) and field (scintillometer) methods (Meijninger, 2003), it was realized that further validation was possible through the use of the NOAA/AVHRR level 1b (LAC) images stored in the satellite active archive (www.saa.noaa.org).

Nowadays remote sensing algorithms for estimating the regional surface fluxes (e.g. evaporation) are widely used. Most of these were developed in the last decade (see e.g. Kustas et al., 1996; Bastiaanssen et al., 1998; Timmermans et al., 2003) and can be applied to imagery of satellites, such as Landsat and AVHRR. For MODIS images evapotranspiration (Nishida et al., 2003) will even be offered as a standard product in the near future. Courault et al. (2004, this volume) give a brief overview of the different available methods. The main advantage of a remote sensing technique is that it can provide regional estimates of the surface energy balance terms, while most conventional techniques are point measurements that are representative of small areas (i.e. source area). Although high-resolution satellites such as LANDSAT (30 m) and ASTER (15 m) are preferable for detailed studies, coarse resolution imagers such as NOAA/AVHRR (1 km at nadir) and MODIS (250–1000 m) have the advantage of almost daily scene coverage and are essentially freely obtainable from the satellite image archives. Therefore these are well suited for agroclimatological monitoring. Moreover, spatially distributed latent heat fluxes can be used specifically for improvement of irrigation water allocation, scheduling, forecasting and evaluation (Droogers et al., 2000; Droogers and Bastiaanssen, 2002).

Recently, validation studies of remote sensing algorithms have been conducted using ground based scintillometer data (Bastiaanssen, 2000; Hemakumara et al., 2002; Lagouarde et al., 2002; Roerink et al., 2000; Watts et al., 2000; Meijninger, 2003). Menenti et al. (2004, this volume) make a validation of the SEBI–SEBS method in different parts of the world. The scintillation method can estimate the sensible heat flux from the propagation statistics of an electromagnetic wave emitted over a certain distance along the surface (see e.g. de Bruin et al., 1995). The advantage of the method is that it can provide surface fluxes of sensible heat at scales comparable to remote sensing methods. For example, Kohsiek et al. (2002) have demonstrated that the scintillation method can be applied over distances up to 10 km. As a result the difference in observational scale between the remote sensing method and the ground observations decreases.

In this study a remote sensing algorithm known as SEBAL (surface energy balance algorithm for land) (Bastiaanssen et al., 1998) is applied to NOAA-14 AVHRR level 1b (LAC) data, which have been downloaded from the satellite active archive (SAA). The algorithm computes most essential hydro-meteorological parameters empirically and requires only little field information (incoming solar radiation, air temperature and wind speed data). The sensible heat flux H is solved iteratively using Monin–Obukhov similarity theory (MOST) and the latent heat flux LE is derived as the closure term of the surface energy balance equation.

$$\mathrm{LE} = (R_\mathrm{n} - G) - H \tag{1}$$

The purpose of this study is to compare the SEBAL-derived sensible heat fluxes with other techniques such as ground based scintillometer and *in-situ* (variance method) surface fluxes from two different sites for a period spanning a growing season (118 days). We have used data from an experiment that took place in the Gediz river basin (Turkey) in 1998 (Kite & Droogers, 2000; Meijninger & de Bruin, 2000). In the next section all three methods are explained. The experimental set-up is described in the section describing the study site, after which the results are presented and discussed.

Materials and methdos

NOAA-14 image processing and atmospheric corrections

The level 1b NOAA-14 AVHRR data were downloaded from the satellite active archive (www.saa.noaa.gov). Images where the study site was too far from nadir (extreme viewing angles) or too cloudy were discarded, resulting in 73 images between day number (DOY) 152 and 277. The images were first resampled to a latitude–longitude grid with a pixel size of 0.01°, basically according to the method by Di & Rundquist (1994). However, the quality of the resampling was much improved through the use of a two-dimensional filter technique rather than the one-dimensional row filter proposed by the latter authors. Di & Rundquist (1994) make corrections for each scan line individually, which often requires interpolation over multi-pixel gaps. If the scan lines are combined in memory, then interpolation across gaps can be made in the most advantageous direction. Geo-correction to within one pixel accuracy was done through the use of digital chart of the world maps of the Turkey coastline. One pixel (0.01° longitude by 0.01° latitude), although not square, corresponds to an area of close to 1 km^2. Although re-sampling to a UTM grid would have been possible, it was decided to resample as little as possible in order to retain the original pixel radiance values as much as possible.

Pre-processing of AVHRR channels 1 and 2 consisted of the conversion of raw counts to percent reflectance values with post-launch NOAA-14 calibration (Rao & Chen, 1996). The thermal channels 4 and 5 were calibrated into radiances and then into brightness temperatures by inverting the Planck function (Cracknell, 1997). All steps described above are implemented in a small computer program (NPR1b), which is available from the lead author on request.

For the narrow-band to broad band albedo conversion using channels 1 and 2 the empirical constants proposed by Valiente et al. (1995) were applied. Finally, the method of Gutman (1988) was used to derive monthly mean surface albedo values in order to correct for the fluctuations in the surface reflectance due to angular variability of the AVHRR sensor and bidirectional effects.

The scintillation and temperature variance methods

The scintillation method is based on the analysis of intensity fluctuations (known as scintillations), of a near-infrared light beam ($\lambda = 0.94\,\mu$m) that has propagated over a horizontal distance (L) between the transmitter and the receiver (see Figures 2 and 3). In this case a large aperture scintillometer (LAS) is used with an aperture diameter (D) of 0.15 m, which makes it possible to measure over distances up to 5 km.

The observed light intensity fluctuations are related to fluctuations of the refractive index of air, which in turn are related to temperature variations (de Bruin et al., 1995; Meijninger, 2003). These can then be related to the sensible heat flux H, which is derived iteratively by applying the Monin–Obukhov similarity theory (MOST). In addition the Bowen ratio appears in the equations. This parameter can be determined with standard meteorological equipment or solved iteratively (Meijninger, 2003). For stable conditions the validity of the scintillation method is uncertain. Therefore, night time flux is set at $-0.5\ R_n$ for estimating the daily average sensible heat flux (H_{24}).

The temperature variance method, a conventional 'point' method, is also based on MOST and can estimate the sensible heat flux from temperature fluctuation measurements (σ_T) collected by a fast response thermocouple (Tillman, 1972).

As is the case with the scintillation method, the validity of the variance method during stable conditions is uncertain. Therefore we followed the same procedure to derive the daily average sensible heat flux and set the sensible heat flux during the night also equal to $-0.5\ R_n$.

Energy balance calculations with SEBAL

In this study the program SHEBA (Delphi Pascal) is used. This program implements the main characteristics of the SEBAL method (surface energy balance algorithm for land, see Bastiaanssen et al., 1998; Bastiaanssen, 2000) but it is specifically designed to be more efficient and faster ($\approx 5\times$) in calculating the sensible heat fluxes (Gieske, 2003). Throughout this paper we will refer to SEBAL to indicate the remote sensing method. The algorithm consists of a number of steps to solve the energy balance for each pixel. Here it is applied to surface albedo, brightness temperature and NDVI (normalised difference vegetation index) maps based on NOAA-14 AVHRR data (channels 1, 2, 4 and 5). The following relation is used to evaluate the surface roughness length for momentum transport z_{om}

$$z_{om} = \exp(c_1 + c_2 \mathrm{NDVI}) \tag{2}$$

The values of the constants c_1 and c_2 depend on local field conditions. Sets of constants, which are different from those taken as default here, can be found for example in Bastiaanssen (2000). The roughness length for heat transport z_{oh} was taken as 0.01. The values of z_{om} and z_{oh} are not critical to the overall procedure to calculate evapotranspiration. The instantaneous net radiation (R_n) is computed from incoming and reflected solar and thermal radiation, where the incoming short wave radiation is taken from the Menemen climate station. The outgoing long wave radiation is computed from the radiometric surface temperature. The incoming long wave radiation is computed from the radiometric surface temperature. The incoming long wave radiation is derived from the air temperature taken from the Menemen climate station and the effective atmospheric emissivity, which in turn is derived from the atmospheric transmittance. The instantaneous soil heat flux (G) is determined according to the empirical relationship proposed by Bastiaanssen et al. (1998). The sensible heat flux for each pixel (H_x) is derived from flux inversion at a selected dry pixel (where $H_{dry} = (R_n - G)_{dry}$) and a wet pixel (where $H_{wet} = 0$ W m^{-2}) inside the image.

The extreme pixels within the image were carefully selected in the Aegean Sea (wet pixel) and north of the city Izmir (dry pixel). The sensible heat flux is solved iteratively applying MOST and using wind speed data that was extrapolated to the blending height and assumed to be constant for the entire image. Finally, the latent heat flux (LE) may be computed as the residual of the surface energy balance equation (Equation 1). However, in order to facilitate comparison with the sensible heat flux, use is made of the instantaneous evaporative fraction Λ, defined as follows:

$$\Lambda = \frac{(R_n - G) - H}{R_n - G} \tag{3}$$

Assuming that the evaporative fraction (Λ) is constant over the day the daily average sensible heat (H_{24}) can be derived from Λ and the daily average net radiation (R_{n24}) as follows

$$H_{24} = (1 - \Lambda)R_{n24} \tag{4}$$

Note that it is also possible to compare the instantaneous sensible heat values H_{LAS} and H_{SEBAL} directly. However, the use of Equation (3) is to be preferred because using integrated daily values smoothes the intrinsic fluctuations in H_{LAS}. Furthermore, errors in the determination of H_{SEBAL} due to errors in the term $R_n - G$, are also partly compensated by the use of Λ as in Equation (2).

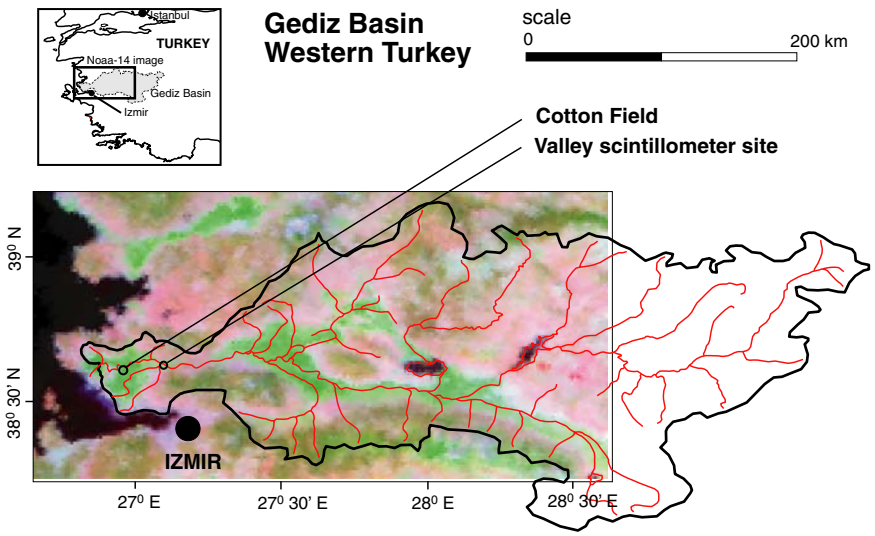

Figure 1. Map of western part of Turkey (left) showing the locations of the cotton field, the LAS set-up in the valley and the Menemen climate station (right). Also a NOAA-14 false colour composite image is shown.

Study site and experimental design

The LAS was deployed across a valley located in the Gediz river basin (Figures 1–3) east of Menemen (western part of Turkey). The path length of the LAS was 2.7 km and the effective height of instrument over the valley was 18 m. The land use in the valley consisted of raisin grape (60%), cotton (15%), fruit trees (15%), pasture (5%) and other trees (5%) (Kite & Droogers, 2000). Other measurements were conducted over an irrigated cotton field located west of Menemen (the distance between both locations is approximately 11 km), which is surrounded by other cotton fields. A small mast with a cup anemometer and a fast thermocouple provided statistics of wind speed and temperature at a height of 3 m. Also a net radiometer and a soil heat flux plate were installed to measure net radiation and soil heat flux. Additional meteorological data (hourly values of temperature, wind speed and global radiation) were taken from the Meteorological station in Menemen. In Figure 1 the locations (cotton field, Menemen climate station, LAS) are shown. More detailed information on the experiment can be found in Meijninger & de Bruin (2000).

Results and discussion

The daily average net radiation from SEBAL is compared with the ground observations in Figure 4. The plotted SEBAL net radiation is the average of

(a)

(b)

Figure 2. (a) The figure shows the LAS receiver in the valley. The transmitter is on the opposite hill slope. (b) The picture shows the irrigated cotton field on September 7, 1998.

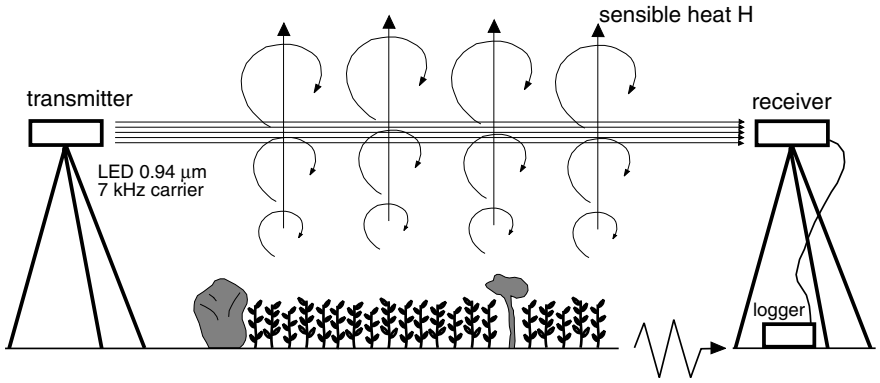

Figure 3. The figure shows the operational principle of a scintillometer. Light from a Light Emitting Diode (LED, 0.94 μm) is bundled into a parallel beam and modulated by a 7 kHz oscillator. At distances of 200 m to several kms the light signal is amplified by a receiver to produce a signal that is representative of changes in the refractive index of the atmosphere. These in turn are caused by the flow of sensible heat from the surface into the atmosphere. The set-up shown here makes use of 3 m high tripods. In practice high towers or hills are often required to measure over undulating terrain and tall trees.

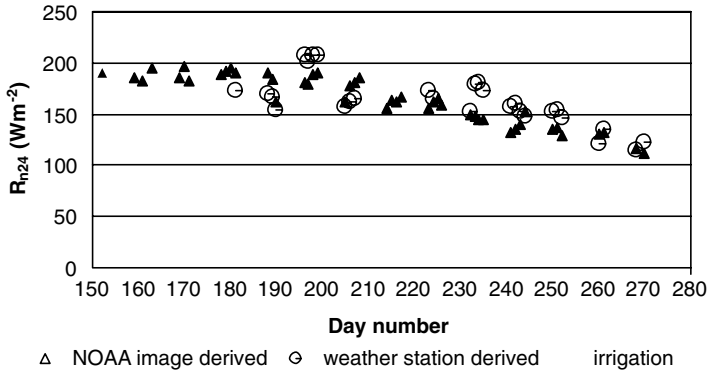

Figure 4. Daily values of R_{n24} plotted against day number. NOAA/SEBAL values are compared with those determined with the weather station on the cotton field. The rectangles indicate the days when the fields were flood-irrigated.

four neighbouring pixels, and spatial variation is below 10 W m^{-2}. A similar analysis was made for the instantaneous measurements (Meijninger, 2003). Most of the scatter in the R_{n24_cotton} is caused by flood-irrigation (see also Figure 5). On days of irrigation and following days ($\sim$4) the ground measurements show a distinctive increase in the net radiation, which is a combined effect of a decrease in the surface albedo and the surface temperature. The raw AVHRR data did not clearly reveal the effects of irrigation because most variation seems to be caused by changes in sun and satellite viewing angles.

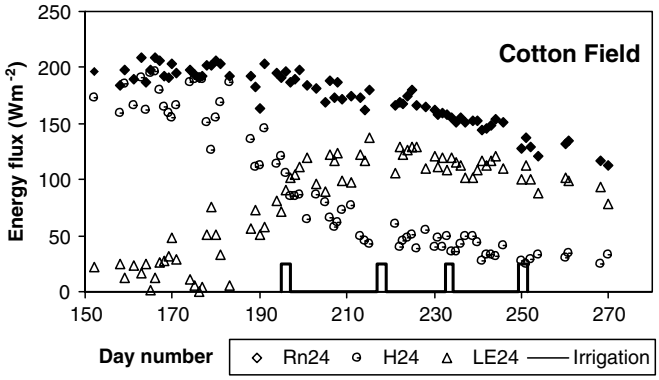

Figure 5. Daily values of net radiation, sensible and latent heat fluxes, derived from the NOAA/SEBAL analysis, plotted against day number. The evapotranspiration increases sharply at the beginning of the flood irrigation, whereas the sensible heat flux decreases.

Daily values of net radiation, sensible and latent heat fluxes, derived from the NOAA/SEBAL analysis, are plotted against day number in Figure 5. The figure shows how evapotranspiration increases sharply at the start of the flood irrigation, whereas the sensible heat flux decreases. The NOAA/SEBAL results for the cotton field shown in the figure are averages of four neighbouring pixels where the spatial variation of the surface flux was generally less than 30 W m^{-2}. Thus the effect of errors in the geo-correction is smoothed. Meijninger (2003) suggests on the basis of the temperature variance method that the sensible heat flux may be overestimated by the NOAA/SEBAL procedures in the initial (non-irrigated) period due to the selection of dry pixels which were not actually dry.

Figure 6 shows the difference in evaporative fraction evolution between the irrigated cotton field area and the more heterogeneous valley. It can be seen that Λ for the valley does not changes dramatically over the season. It should be noted that the valley is only about 2 km wide at the location of the LAS instrument. Hence there are at best only two pixels, which can be compared to the situation in the valley floor. Often pixels represent both valley and hill slope areas. Moreover, maximum resolution only occurs when the study area is in the nadir position of the NOAA images. Away from this the resolution decreases from 1 to 4 km near the edges.

Figure 7 shows the evapotranspiration sequence according to the NOAA/SEBAL processing in the cotton field area together with the values obtained through the temperature variance method. The values reported by Kite & Droogers (2000) have been indicated for comparison as follows: (1) biophysical (2) FAO-24 (3) feedback NOAA (4) feedback Landsat (5) FAO-56 dual K_c method (6) SEBAL Landsat (7) SWAP (8) SLURP. More

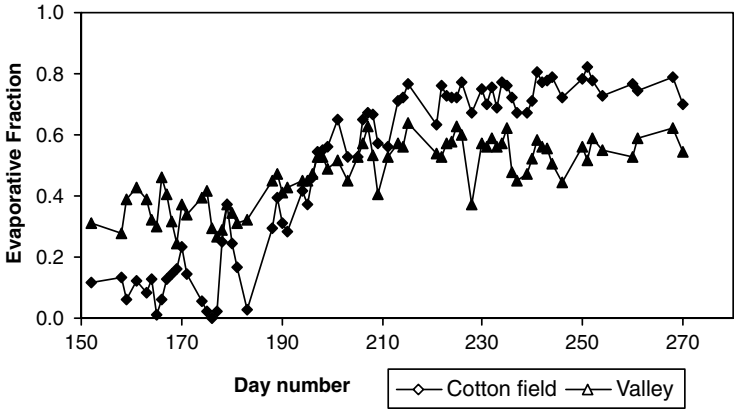

Figure 6. The figure shows the change in evaporative fraction Λ for both the homogeneous cotton area and the more heterogeneous valley area.

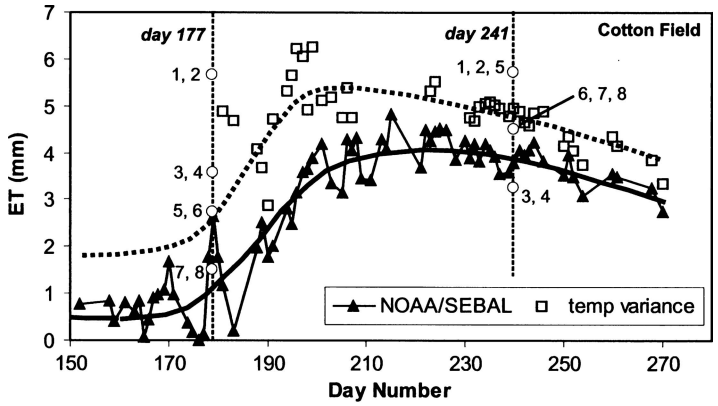

Figure 7. The evapotranspiration sequence according to the NOAA/SEBAL and temperature variance processing in the cotton field area. For comparison the values reported by Kitea & Droogers (2000) have been indicated as follows: (1) biophysical (2) FAO-24 (3) feedback NOAA (4) feedback Landsat (5) FAO-56 (6) SEBAL Landsat (7) SWAP (8) SLURP.

details on these methods may be found in special issue 229 of the Journal of Hydrology. Note that the evapotranspiration for the cotton field on August 29 should be 4.5 mm according to Kite & Droogers (2000). Figure 7 indicates the large range of reported results. Considering both days 177 and 241 the overall NOAA results seem to agree most with methods (7) and (8), although on day 241 there is also good agreement with the SEBAL Landsat method (6). Clear outliers are methods (1)–(3). One should note also that an evapotranspiration of 6 mm corresponds to an energy flux of 170 W m^{-2}, which is near the maximum available energy according to Figures 4 and 5.

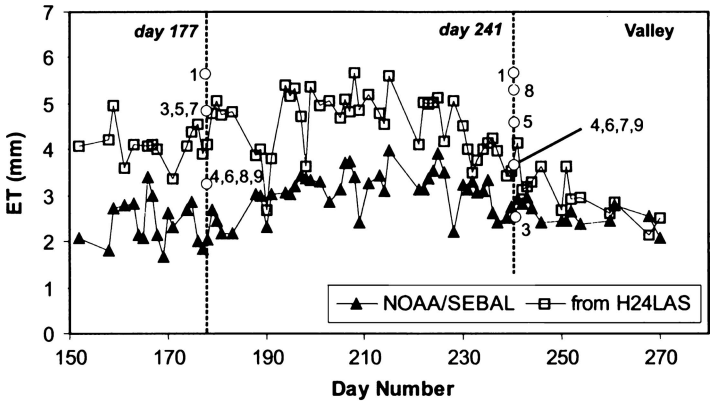

Figure 8. The evapotranspiration sequence according to the NOAA/SEBAL and HLAS processing in the valley area. For comparison the values reported by Kite & Droogers (2000) have been indicated as follows: (1) biophysical (3) feedback NOAA (4) feedback Landsat (5) FAO-56 (6) SEBAL Landsat (7) SWAP (8) SLURP (9) LAS scintillometer.

Figure 8 shows the development of the evapotranspiration in the valley according to the NOAA/SEBAL processing and according to the scintillometer results. Use is made of the NOAA-derived daily net radiation R_{n24} received by the valley surface. It was found that R_{n24} data correspond very well with the data of the cotton field area, which in turn highly correlate with the weather station data at that location (Figures 4 and 5). Therefore we could put $ET_{LAS} = R_{n24} - H_{24LAS}$, whereas ET_{NOAA} was obtained as $(1 - \Lambda)R_{n24}$. For comparison the values reported by Kite & Droogers (2000) have also been indicated in the figure. One explanation for the difference between ET_{LAS} and ET_{NOAA} may perhaps be the following: ET_{NOAA} is derived using the instantaneous evaporative fraction Λ, which is assumed to remain constant during the day. During days of near-ideal conditions (no clouds, clear sky, calm conditions) this appears to be a fair assumption (see also the discussion in Meijninger, 2003). The ETLAS on the other hand is determined through the use of integrated values of instantaneous HLAS observations, where conditions are normally not ideal.

Therefore H_{24LAS} is normally lower than what one would expect under "ideal" conditions and then ET_{LAS} is higher. Conversely when conditions are ideal, one would expect the methods to agree. Inspection of the two graphs in Figure 8 shows that this might be the case for a couple of isolated days in the initial period, and more consistently towards the end of the study period. The LAS results would then correspond more to actual field conditions, whereas the NOAA/SEBAL results would reflect the evapotranspiration that would occur if the evaporative fraction remained constant during the day. One should note as mentioned before, that the small size valley conditions are

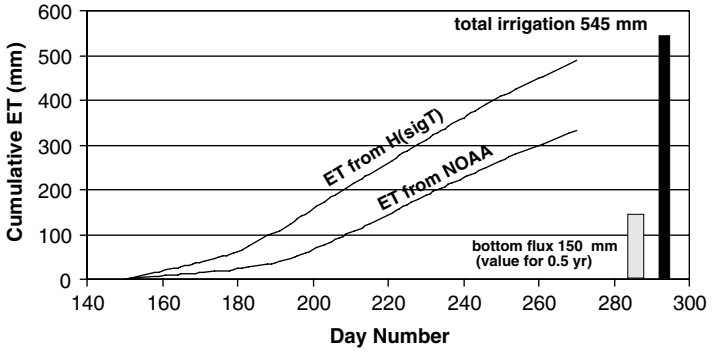

Figure 9. Cumulative ET values calculated for both the temperature variance H(sigT) and the NOAA/SEBAL methods in the cotton field area. The figure also indicates total irrigation (545 mm) and estimated bottom flux (150 mm) according to Droogers & Bastiaanssen (2002).

not well suited for NOAA modelling. Apart from the pixel composition and size problem, there may also be micrometerological complications due to, for example, air circulation through the valley, that would violate the SEBAL assumptions.

Figure 9 indicates the cumulative values of the ET calculated by both the NOAA/SEBAL and H(sigT) methods, from day 150 (May 30) to day 270 (September 28). The figure also shows the total irrigation of 545 mm (Droogers & Bastiaanssen, 2002), and an estimated half-year bottom flux of 150 mm. There was no rain in this period. The cumulative plotting removes the day-to-day errors in the determination of the ET, and reveals the systematic differences between the methods much better. The ultimate test for the satellite methods is whether good agreement can be reached on a seasonal basis with results obtained from careful analysis of all water balance components in areas such as the cotton irrigation area described here.

Conclusions

In this study surface flux maps of sensible heat generated by a satellite remote sensing technique (NOAA/SEBAL) have been compared with ground observations. The ground measurements were conducted at two different locations, in a homogeneous cotton field area and in a more heterogeneous valley, about 2 km wide. The daily net radiation values obtained through the NOAA/SEBAL modelling are in good agreement with those observed in the cotton field area. The instantaneous latent and sensible heat fluxes provided by NOAA/SEBAL correspond well with the ground measurements for the cotton site over the entire growing season. However, Meijninger (2003) noted

that daily fluxes obtained from the temperature variance method deviated somewhat from those obtained by the NOAA/SEBAL series for the first part of the period. For the valley site, where the LAS was installed, the results show a larger discrepancy. The spatial coverage of the LAS (i.e source area) in the heterogeneous valley may have been too small compared to the spatial resolution of the AVHRR images. Furthermore, we suspect that the valley is too narrow for the AVHRR's spatial resolution, leading to pixels of mixed composition. However, another explanation may be that the ET_{LAS} calculation is based on integrated measurements of the sensible heat flux during the day, whereas the SEBAL methods operates on the assumption of a constant evaporative fraction. Under "ideal" conditions the results of the two methods would converge. Another problem (Meijninger, 2003) could perhaps be caused by difficulties in identifying dry pixels in the area, especially in the first part of the study period, leading to overestimation of the sensible heat flux. Work is underway to validate satellite remote sensing techniques using longer scintillometer path lengths up to 10 km using the XLAS (Kohsiek et al., 2002), which allows a better comparison with the low-resolution satellites (NOAA/AVHRR, METEOSAT MSG). Furthermore, a satellite-scintillation combination will be investigated where relative extreme 'scintillometer' pixels will be used to apply SEBAL to areas where wet and dry pixels are not present. Notwithstanding these difficulties, however, the present study has shown that highly detailed time series of evapotranspiration are possible with the present state of NOAA/AVHRR archives and techniques. Finally, crop ET can be directly calculated with the SEBAL method, and therefore there is no longer any need to apply crop factors.

Acknowledgements

We are grateful for the critical notes and suggestions of the referees.

References

Bastiaanssen, W.G.M., Menenti, M., Feddes, R.A. & Holtslag, A.A.M. 1998. A remote sensing surface energy balance algorithm for land (SEBAL) – 1. Formulation. *Journal of Hydrology* 212–213: 198–212.

Bastiaanssen, W.G.M. 2000. SEBAL-based sensible and latent heat fluxes in the irrigated Gediz Basin, Turkey. *Journal of Hydrology* 229: 87–100.

Courault, D., Seguin, B. & Olioso, A. 2003. Review to estimate evapotranspiration from remote sensing data: Some examples from the simplified relationship to the use of mesoscale atmospheric models. *ICID Workshop on Remote Sensing of ET for Large Regions*, 17 September 2003, Montpellier, France (this volume).

Cracknell, A.P. 1997. *The Advanced Very High Resolution Radiometer (AVHRR)* (968 pp). Taylor & Francis Ltd., UK.

de Bruin, H.A.R., van den Hurk, B.J.J.M. & Kohsiek, W. 1995. The scintillation method tested over a dry vineyard area. *Boundary-Layer Meteorology* 76: 25–40.

Di L. & Rundquist, D.C. 1994. A one-step algorithm for correction and calibration of AVHRR level 1b data. *Photogrammetric Engineering and Remote Sensing* 60(2): 165–171.

Droogers, P., Bastiaanssen, W.G.M., Beyazgul, M., Karyam, Y., Kite, G.W. & Murray-Rust, H. 2002. Distributed agro-hydrological modeling of an irrigation system in western Turkey. *Agricultural Water Management* 43: 183–202.

Droogers, P. & Bastiaanssen, W. 2002. Irrigation performance using hydrological and remote sensing modeling. *Journal of Irrigation and Drainage Engineering* 128(1): 11–18.

Gieske, A. 2003. The iterative flux-profile method for remote sensing applications. *International Journal of Remote Sensing* 24(16): 3291–3310.

Gutman, G. 1988. A simple method for estimating monthly mean albedo of land surfaces from AVHRR data. *Journal of Applied Meteorology* 27: 973–988.

Hemakumara, H.M., Chandrapala, L. & Moene, A.F. 2002. Evapotranspiration fluxes over mixed vegetation areas measured from a large aperture scintillometer. *Agricultural Water Management* 58: 109–122.

Kite, G.W. & Droogers, P. 2000. Comparing evapotranspiration estimates from satellites, hydrological models and field data. *Journal of Hydrology* 229: 3–18.

Kohsiek, W., Meijninger, W.M.L., Moene, A.F., Heusinkveld, B.G., Hartogensis, O.K., Hillen, W.C.A.M. & De Bruin, H.A.R. 2002. An extra large aperture scintillometer (XLAS) with a 9.8 km path length. *Boundary-Layer Meteorology* 105: 119–127.

Kustas, W.P., Humes, K.S., Norman, J.M. & Moran, M.S. 1996. Single- and dual-source modelling of surface energy fluxes with radiometric surface temperature. *Journal of Applied Meteorology* 35: 110–121.

Lagouarde, J.-P., Jacob, F., Gu, X.-F., Oliso, A., Bonnefond, J.-M., Kerr, Y., McAneny, K. & Irvine, M. 2002. Spatialization of sensible heat flux over a heterogeneous landscape. *Agronomie* 22: 627–633.

Meijninger, W.M.L. & De Bruin, H.A.R. 2000. The sensible heat fluxes over irrigated areas in western turkey determined with a large aperture scintillometer. *Journal of Hydrology* 229: 42–49.

Meijninger, W.M.L. 2003. *Surface Fluxes over Natural Landscapes using Scintillometry* (164 pp). Ph D Dissertation, Wageningen University, The Netherlands.

Menenti, M., Jia, L. & Su, Z. 2003. On SEBI-SEBS validation in France, Italy, Spain, USA and China. *ICID Workshop on Remote Sensing of ET for Large Regions*, 17 September 2003, Montpellier, France (this volume).

Nishida, K., Nemani, R.R., Running, S.W. & Glassy, J.M. 2003. An operational remote sensing algorithm of land surface evaporation. *Journal of Geophysical Research* 108(D9): 4270.

Rao, C.R.N. & Chen, J. 1996. Post-launch calibration of the visible and near-infrared channels of the advanced very high resolution radiometer on the NOAA-14 spacecraft. *International Journal of Remote Sensing* 17: 2743–2747.

Roerink, G.J., Su, Z. & Menenti, M. 2000. S-SEBI: A simple remote sensing algorithm to estimate the surface energy balance. *Physics and Chemistry of the Earth* 25: 147–157.

Tillman, J.E. 1972. The indirect determination of stability, heat, and momentum fluxes in the atmospheric boundary layer from simple scalar variables during unstable conditions. *Journal of Applied Meteorology* 11: 783–792.

Timmermans, W.J., Gieske, A.S.M., Wolski, P., Arneth, A. & Parodi, G.N. 2003. Determination of water and heat fluxes with MODIS imagery – Maun, Botswana. *SPIE Annual Conference*, Barcelona, 7–12 September 2003.

Valiente, J.A., Nunez, M., Lopez-Baeza, E. & Moreno, J.F. 1995. Narrow-band to broad-band conversion of meteosat visible channel and broad-band albedo using both AVHRR-1 and-2 channels. *International Journal of Remote Sensing* 16(6): 1147–1166.

Watts, C.J., Chebouni, A., Rodriguez, J.-C., Kerr, Y.H., Hartogensis, O. & De Bruin, H.A.R. 2000. Comparison of sensible heat flux estimates using AVHRR with scintillometer measurements over semi-arid grassland in Northwest Mexico. *Agricultural and Forest Meterology* 105: 81–89.